Letter

High-fidelity multiphoton-entangled cluster state with solid-state quantum emitters in photonic nanostructures

Konstantin Tiurev,* Martin Hayhurst Appel, Pol Llopart Mirambell, Mikkel Bloch Lauritzen, Alexey Tiranov, Peter Lodahl, and Anders Søndberg Sørensen

Center for Hybrid Quantum Networks (Hy-Q), The Niels Bohr Institute, University of Copenhagen, DK-2100 Copenhagen Ø, Denmark

(Received 16 July 2020; revised 16 November 2021; accepted 11 February 2022; published 2 March 2022)

We propose a complete architecture for deterministic generation of entangled multiphoton states. Our approach utilizes periodic driving of a quantum-dot emitter and an efficient light-matter interface enabled by a photonic crystal waveguide. We assess the quality of the photonic states produced from a real system by including all intrinsic experimental imperfections. Importantly, the protocol is robust against the nuclear spin bath dynamics due to a naturally built-in refocusing method reminiscent to spin echo. We demonstrate the feasibility of producing Greenberger-Horne-Zeilinger and one-dimensional cluster states with fidelities and generation rates exceeding those achieved with conventional "fusion" methods in current state-of-the-art experiments. The proposed hardware constitutes a scalable and resource-efficient approach towards implementation of measurement-based quantum computing and quantum communication.

DOI: 10.1103/PhysRevA.105.L030601

The development of efficient sources of on-demand entangled photons is an ongoing experimental endeavour. Quantum states containing large numbers of entangled photons is a desirable component for many quantum-information processing applications, including photonic quantum computing [1–6], quantum simulations [7,8], entanglement-enhanced metrology [9,10], and long-distance quantum communication [11–16]. Furthermore, access to high-fidelity multiphoton entanglement would have applications for fundamental tests of quantum mechanics [17–19].

The creation of entangled states containing large numbers of photons is, however, a formidable challenge due to the lack of deterministic and scalable methods for the production of such states. Spontaneous parametric downconversion (SPDC) sources [20–22] combined with interference between generated pairs and single-photon detection [23–25] have been implemented to scale up the number of entangled photons [3,26–30] with a recent state-of-the art experiment demonstrating genuine 12-photon entanglement [31]. Today, scaling up is pursued also commercially by multiplexing many probabilistic SPDC sources towards photonic quantum computing [5,6]. An alternative and much less investigated strategy is to apply on-demand photon emission from a single quantum emitter. In this case, a single spin in the emitter serves as the entangler of consecutively emitted photons [13–15,32–36] and combined with photonic nanostructures for enhancing photon-emitter coupling [37], long strings of highly entangled photons could potentially be generated. A proof-of-concept experiment with quantum dots (QDs) in bulk samples recently demonstrated three-qubit linear cluster states [38]. However, it is an open question how these deterministic sources can be scaled up in a real experimental setting.

In the present Letter we develop a complete architecture for deterministic generation of time-bin entangled multiphoton states. Our proposal exploits a QD emitter embedded in a photonic nanostructure and removes the dominant noise source through a built-in spin-echo protocol. We investigate the performance of the architecture, taking into account all intrinsic imperfections and identify the governing physical processes and figures of merit, hence, providing a path for scaling up the protocol. Our results demonstrate that recent experimental advances make QDs in photonic nanostructures highly promising sources of scalable multiphoton entangled states.

Self-assembled semiconductor QDs have lately seen remarkable experimental progress, opening new possibilities for photonic quantum technologies. Particularly, spin qubits realized with a single charge injected into the QD enable efficient coherent light-matter interfaces and control over emitted photons due to simultaneously achievable high photon generation rate, good optical and spin coherence properties [37,39–41], and near-perfect spin rotations [42]. Integration of QDs into photonic nanostructures, such as photonic crystal waveguides (PCW), significantly improves the quality of quantum interfaces and has resulted in single-photon indistinguishability (I) of two subsequently emitted photons exceeding 96% [37,43–47], an internal efficiency β exceeding 98% [48], and on-demand entangled photon sources with higher than 90% state fidelity [49]. Recently it was demonstrated that these sources can be scaled up to reach the threshold for quantum advantage [50].

The proposed architecture based on a QD containing a hole spin in a PCW is illustrated in Fig. 1. It relies on encoding photonic qubits in separate time bins corresponding to early ($|e\rangle$) or late ($|l\rangle$) arrival times. The general idea is to repeatedly apply the pulse sequence of Fig. 1(b) to coherently control a ground-state spin in the QD and emit single photons on the targeted optical transition in the designated time bin.

*konstantin.tiurev@gmail.com

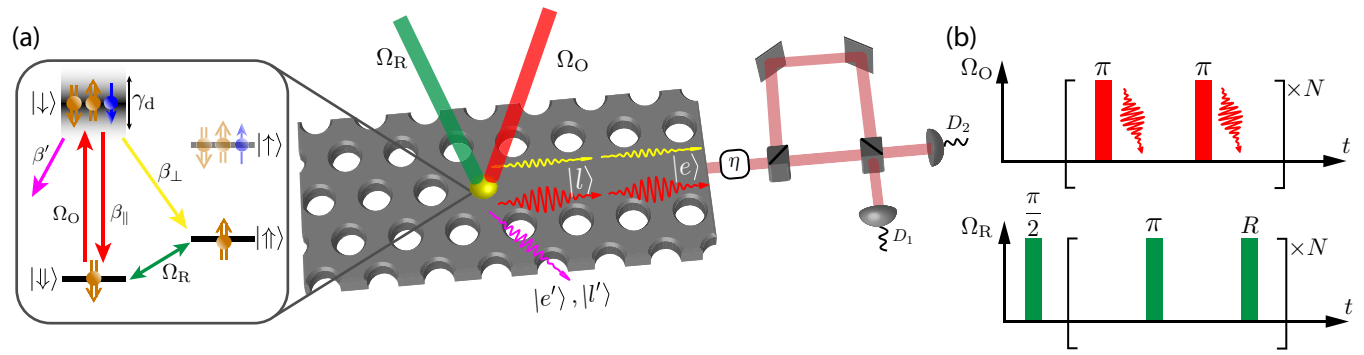

FIG. 1. Architecture for generation and measurement of time-bin entangled photons. (a) Center: Light-matter interface based on a QD (yellow dot) placed in a PCW formed of semiconductor with a periodic dielectric structure. Driven cyclically by excitation pulses Ω_O (red beam) and rotation pulses Ω_R (green beam), a QD emits entangled photonic qubits in either the early or the late temporal mode. The inset: Energy-level structure of a positively charged QD consisting of hole spin states $|\Uparrow\rangle$ and $|\Downarrow\rangle$ and trion states $|\uparrow\rangle$ and $|\downarrow\rangle$. Upon spontaneous emission, an early ($|e\rangle$) or a late ($|l\rangle$) photon is emitted into the PCW on either the vertical transition (red decay path in the inset, red wave in the PCW)or on the undesired diagonal transition (yellow decay path, yellow wave). Additionally, an early ($|e'\rangle$) or a late ($|l'\rangle$) photon can be emitted out of the waveguide mode and thereby lost (purple decay path, purple wave). The PCW simultaneously ensures a high internal efficiency $\beta_\parallel + \beta_\perp$ as well as a high selectivity of the vertical decay path. Right: Setup for detection of time-bin entangled photons. Passing photons through a single interferometer arm yields a Z measurement whereas interfering the early and late photons at the final beam splitter yields a measurement in the X or Y basis. Active optical routing can be implemented with free space resonant electro-optic modulators, enabling low loss state characterization. Realistically the repetition rate can be made compatible with the maximally achievable generation rate, which is limited by the spin rotation time and/or the decay rate of the quantum dot. Alternatively, passive routing can be implemented using standard beam splitters at the expense of not being able to freely chose the measurement basis. η represents the total measurement efficiency. (b) Sequence of pulses Ω_O and Ω_R used to generate time-bin-encoded entangled photonic states. Optical pulses Ω_O are used to excite a transition $|\Downarrow\rangle \rightarrow |\downarrow\rangle$ with radiative decay rate γ, whereas the ground-state rotations Ω_R are realized with Raman transitions

Initially the hole spin is prepared in a superposition of the two spin states $|\Downarrow\rangle$ and $|\Uparrow\rangle$ using a $\pi/2$ pulse from the Raman field Ω_R. Within each round of the protocol the QD is first excited to the trion state $|\downarrow\rangle$ using the optical field Ω_O if the QD is in $|\Downarrow\rangle$. From the trion state the QD decays emitting an early photon $|e\rangle$. Subsequently, the hole spins states are flipped using a Raman π pulse followed by excitation with Ω_O and emission of a late photon $|l\rangle$. This procedure creates an entangled state between the spin and the time bin of the outgoing photon, which can be extended to multiple photons by repeating the protocol with a spin rotation R between each round of the protocol. The nature of the entangled state is defined by the choice of R: $R = \pi$ creates the Greenberger-Horne-Zeilinger (GHZ) state [51] whereas $R = \pi/2$ creates the one-dimensional cluster state [52]. The states are, subsequently, analyzed using the interferometric setup shown in Fig. 1(a). Here the early part of the photon is redirected to the long arm so that it interferes with a late photon taking the short arm. This, thus, enables projective measurement onto superpositions of early and late time bins.

Multiple other schemes for the generation of cluster states from QDs have previously been considered. As such, Refs. [33,38,53] exploited polarization selection rules to achieve spin-photon entanglement instead of our time-bin encoding. Reference [38] relied on the natural splitting between two dark-exciton states to achieve rotation between the internal states. This meant that the splitting could not be controlled, and the decay of the dark excitons limited the number of photons that could be emitted. Instead Refs. [33,53] considered two stable ground states split by an applied magnetic field. In this case the applied magnetic field changes the polarization selection rules. This introduces an error in the protocol and reduces the photon indistinguishability unless the magnetic field is kept very low, which slows down the protocol leading to decoherence. We overcome this problem by performing spin rotation using pulses, which can be turned on and off, thus, not affecting the dynamics during the decay.

A protocol for entangling photons in their time-bin degree of freedom has been considered experimentally in Ref. [34] using a QD in a micropillar cavity. That work, however, was unable to generate entanglement due to the inability to drive spin rotations whereas having cycling optical transition. A similar scheme implemented with nitrogen-vacancy centers in diamond [54] has been used to demonstrate entanglement limited to two particles due to the low-photon collection efficiency and long initialization times. Our proposal solves these problems by embedding a quantum dot into a photonic crystal waveguide. As shown in a recent experiment [55], high-quality optical cyclings can be induced on the designated transition due to the high coupling asymmetry of the two in-plane linear dipole transitions. In combination with ground-state spin rotations, this is the basis for the efficient scaling of the protocol. In the following, we prove and benchmark the scalability of the approach by evaluating the fidelity of multiphoton GHZ and cluster states in the presence of all relevant imperfections.

We assess the quality of the spin-multiphoton state by calculating the infidelity [52] $\mathcal{E}^{(N)} = 1 - \mathrm{Tr}_{\mathrm{env}}\{\langle\Psi|\,\hat{\rho}^{(N)}\,|\Psi\rangle\}$, where $\hat{\rho}^{(N)}$ is the density operator of an N-photon state affected by imperfections, $|\Psi\rangle$ is the target state, and $\mathrm{Tr}_{\mathrm{env}}$ denotes a trace over the emission time and unobserved degrees of freedom, such as phonons or lost photons. Photonic quantum-information protocols, e.g, for quantum communication [11–15] or computation [58,59] are typically designed

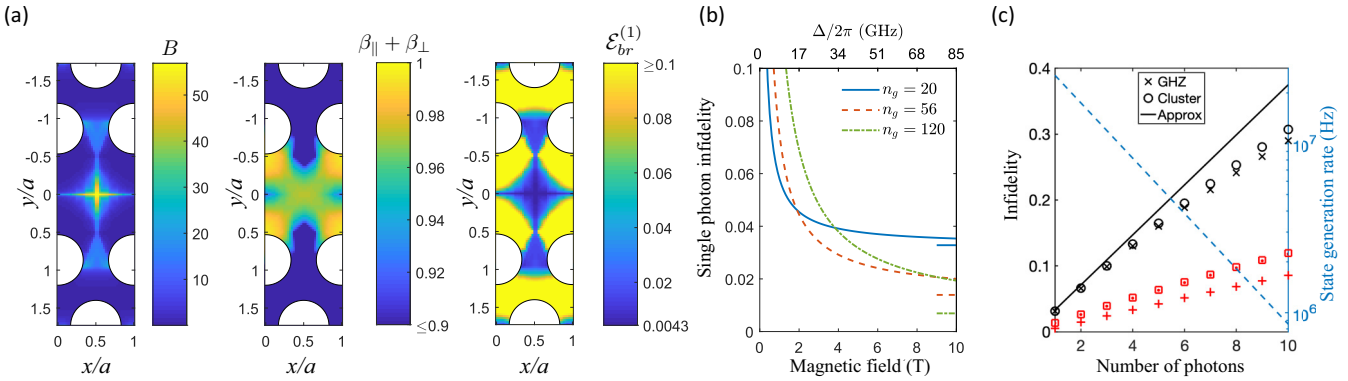

FIG. 2. (a) Spatial map of the optical branching ratio asymmetry B (left), total coupling efficiency into the mode of the waveguide $\beta_\parallel + \beta_\perp$ (center), and the infidelity of the spin-photon entangled state due to the spatially varying branching ratio (right) within the unit cell of size a of the PCW for $n_g = 20$. (b) Infidelity of spin-photon entangled states versus the applied magnetic field (detuning Δ corresponding to a g-factor of $|g| = |g_e| + |g_h| = 0.6$ [56]) for various group indices n_g attributed to different spectral positions with respect to the band gap of the PCW. Straight lines on the right mark the infidelities in the limit $\Delta \to \infty$. For each n_g, γ is evaluated using the simulated Purcell factor assuming a bulk rate of $\gamma_{\text{bulk}} = 1\ \text{ns}^{-1}$ [37]. (c) Total infidelity versus number of photons with all imperfections taken into account and $n_g = 56$. The solid line shows the infidelity in the first-order approximation (1), whereas the black symbols are beyond perturbation theory [52]. Red symbols show the different contributions in Eq. (1), i.e., dephasing $\mathcal{E}_{\text{ph}}$ ($\cdot$), excitation errors $\mathcal{E}_{\text{exc}}$ ($\square$), and imperfect branching $\mathcal{E}_{\text{br}}$ ($+$). The dashed line shows the state generation rate for an outcoupling efficiency $\eta = 0.84$ [50] and a cycle length $T_{\text{cycle}} = 27$ ns [55] compatible with the parameters of Ref. [57]. See the main text for other parameters.

to be loss tolerant by postselecting events without photon loss. In this case the relevant quantity is the fidelity conditioned on the detection of, at least, one photon in either the early or late time bin. The conditional infidelity for the generation of an entangled GHZ or cluster state containing N photons and the spin is in first-order perturbation theory given by [52]

$$\mathcal{E}^{(N)} = N\left(\frac{1-I}{2} + \frac{\sqrt{3}\pi}{8}\frac{\gamma}{\Delta} + \frac{1}{2(B+1)}\right) - \frac{1}{4(B+1)}. \tag{1}$$

Here the spontaneous emission rate γ, the branching ratio B, the degree of indistinguishability I, and detuning of the off-resonant transition Δ are parameters that will be explained below. The second figure of merit for any quantum-information protocol is the overall success probability, which is predominantly determined by the collection efficiency η of the photons. Protocols for photonic quantum-information processing, such as Refs. [11–15,58,59], are typically designed to have some protection against photon loss. The efficiency of a particular protocol in the presence of losses or the amount of losses it can tolerate varies greatly from one protocol to another, but they still work even in the presence of loss. The efficiency is, however, a separate issue from the quality of a state, which we focus on here.

The ideal protocol assumes that only the vertical decay path $|\downarrow\rangle \to |\Downarrow\rangle$ in Fig. 1(a) is allowed such that the excitation and decay form a closed cycle. A finite probability of the diagonal transition $|\downarrow\rangle \to |\Uparrow\rangle$ will lead to an incorrect spin configuration and a reduction of the fidelity. We characterize the cyclicity with a branching parameter $B = (\beta_\parallel + \beta'_\parallel)/(\beta_\perp + \beta'_\perp)$, where $\beta_\parallel(\beta_\perp)$ and $\beta'_\parallel(\beta'_\perp)$ are the probabilities of the vertical (diagonal) transitions into and out of the waveguide mode, respectively. The performance of an experiment will, therefore, rely on the high selectivity of the vertical transitions, i.e., $B \gg 1$.

Using an out-of-plane magnetic field (Faraday configuration) would almost fully eliminate the diagonal transitions due to the selection rules and, therefore, allow for near-perfect branching conditions, but would at the same time prohibit the coherent ground-state Raman transition Ω_{R}, which the protocol depends upon. Instead, we consider an in-plane magnetic field (Voigt geometry) which provides $B = 1$ in bulk but, crucially, allows all-optical spin control. B may then be increased by selectively enhancing the desired optical transition with a photonic nanostructure [34,55,60–62]. This, in combination with the orthogonally polarised linear dipoles of a QD in the Voigt geometry, allows a greatly enhanced B whereas simultaneously retaining the possibility of ground-state spin rotations. In Fig. 2(a) we show calculated β factors and branching ratios B based on the field distribution calculated in Ref. [63]. For a realistic group index $n_g = 20$, which specifies the PCW-induced slow-down factor, a branching ratio of $B > 50$ and an internal efficiency $\beta > 96\%$ are simultaneously achievable by placing a QD in the center of a PCW. To further suppress the residual contribution of the diagonal transitions, we consider frequency filters which can be implemented without introducing significant loss [50] using, e.g., narrow bandpass external (i.e., off-chip) etalons. Assuming high-efficiency filtering of the off-resonant photons, we derive [52] the first-order infidelity due to imperfect branching $\mathcal{E}_{\text{br}}^{(N)} = (N - 1/2)/[2(B+1)]$, which corresponds to the last two terms in Eq. (1) and is shown in Fig. 2(a) for a single emitted photon. For the optimal QD position the single-photon branching infidelity can be lower than 1%.

Next, we consider the effect of dephasing omnipresent in solid-state systems. Decoherence appears through a variety of mechanisms characterized by widely different timescales. As discussed below the protocol is remarkably insensitive to slowly varying processes. On the other hand, phonon scattering appears on timescales (∼picoseconds) shorter than the lifetime of the excited trion state (∼nanoseconds) and

determines the indistinguishability of emitted photons [64–67]. Pure dephasing broadens the zero-phonon line, resulting in the indistinguishability of emitted photons $I = \gamma/(\gamma + 2\gamma_d)$, where γ_d is the phonon-induced dephasing rate [64]. The same mechanism increases the state infidelity, which can, hence, be expressed through the experimentally measurable indistinguishability I as $\mathcal{E}_{\rm ph}^{(N)} = N(1-I)/2$, corresponding to the first term in Eq. (1).

Furthermore, we discuss imperfect operations during the driving pulses. Since the excited trion comprises two Zeeman states [Fig. 1(a)], excitation of undesired transitions have to be suppressed. This is ensured by a large detuning Δ of the off-resonant transition $|\uparrow\rangle \leftrightarrow |\Uparrow\rangle$ compared to the decay rate γ of the $|\downarrow\rangle \leftrightarrow |\Downarrow\rangle$ transition. The detuning can be controlled by a magnetic field, whereas γ can be controlled via the Purcell effect of the waveguide. The probability of off-resonant excitations is strongly suppressed when the system is driven with long and low-intensity laser pulses. On the other hand for long pulses there is a large probability for the desired $|\downarrow\rangle \leftrightarrow |\Downarrow\rangle$ transition to decay and be reexcited during the pulse. The duration of the pulse should, thus, be optimized to suppress the errors. We have evaluated [52] the infidelities corresponding to the optimal driving regimes for both Gaussian and square-shape pulses. The latter allows for a simple analytical expression $\mathcal{E}_{\rm exc}^{(N)} = N\sqrt{3}\pi\gamma/(8\Delta)$, which also represents a good approximation for Gaussian pulses. Additional errors occur if the excitation laser drives the cross transitions $|\Uparrow\rangle \leftrightarrow |\downarrow\rangle$ and $|\Downarrow\rangle \leftrightarrow |\uparrow\rangle$, which, however, can be completely avoided by correct laser polarization in side channel excitation. This is readily implementable in the waveguide geometry [50] but has not yet been implemented in micropillar [62] or planar cavities [60,61], which rely on cross excitation schemes.

Finally, we consider dephasing induced by slow drifts of the energy levels. A particular example arises from the hyperfine interaction between the coherent spin and the slowly fluctuating nuclear spin environment, i.e., the Overhauser noise [68,69], which manifests itself in relatively short ground-state spin coherence times T_2^* [70]. Strikingly, our protocol for time-bin photon generation is insensitive to dephasing induced by such mechanisms because the pulse sequence of Fig. 1(b) flips the ground-states $|\Uparrow\rangle$ and $|\Downarrow\rangle$ between the early and late photons. We assume that the photons are, subsequently, analyzed using the measurement setup of Fig. 1(a), which interferes pulses delayed by a time equal to the time difference between the two excitation pulses. Since the interfered components have spent exactly the same amount of time in the excited states for the early and late parts, our protocol inherently implements a perfect spin-echo sequence [71] at each cycle of the protocol without the need for any additional refocusing methods. Slow drifts of the central frequency of the transition will, hence, not have any influence on the interference. Consequently, either hole or electron spins can be used on an equal basis, even though the latter has a much shorter coherence time T_2^*. On longer times, slow fluctuations of the environment build up to a so-called T_2 noise. However, due to a periodically applied spin-echo sequence this typically happens on timescales [72,73] two orders of magnitude longer than the length of a cycle $T_{\rm cycle}$ [74]. At magnetic fields above approximately 1.5 T, the T_2 noise adds an error $\propto (T_{\rm cycle}/T_2)^n$ with $n \geqslant 1$ negligible compared to other imperfections. It is desirable to avoid magnetic fields below 1.5 T as these allow a highly nontrivial interaction between the QD spin and the Overhauser field [75] which leads to imperfect spin-echo and reduced coherence times.

The insensitivity to slow fluctuations is linked to the measurement setup in Fig. 1(a) where pulses from a single QD are interfered but does not apply if, e.g., attempting to fuse cluster states emitted by different QDs [23–25]. Nevertheless it captures several interesting situations. The quantum repeater protocol of Borregaard *et al.* [15] exploits a single emitter to produce entangled states containing hundreds of photons. Of these, only one photon is interfered with a different emitter, whereas the remaining $N-1$ photons are measured using the setup in Fig. 1(a) and, hence, fulfill the effective spin-echo conditions. Similarly, the protocol of Pichler *et al.* [76] for universal quantum computation using cluster states relies on the emission from a single emitter. We, thus, expect a similar robustness.

A full assessment of the experimental photon generation protocol would also need to take into consideration laser-induced spin relaxation during optical control of the quantum dot as observed in Refs. [42,55]. The precise origin of this effect is not known, but it is believed to be extrinsic to the QDs. Thus, it does not represent an inherent error in our protocol and is not included in our analysis.

All error terms in Eq. (1) depend on the group index of the waveguide: A high n_g increases the decay rate γ and, hence, the indistinguishability but at the same time results in stronger driving of off-resonant transition. Furthermore, the branching ratio can also be improved by the enhancement of n_g. The waveguide, therefore, can be used to control the trade-off between errors and optimize the output state. As shown in Fig. 2(b), a high n_g becomes beneficial given sufficient Zeeman splitting, i.e., for a strong magnetic field or large g-factor [56,77,78]. By engineering the photonic crystal band gap and increasing the group indices to higher values, the single spin-photon infidelity can be reduced to the levels of $\approx 0.5\%$ for sufficiently strong magnetic fields as shown in Fig. 2(b). For more modest magnetic fields, a spin-photon entangled state fidelity above 95% can be reached.

The case of $N = 3$ is of special importance since it potentially serves as a building block for photonic quantum protocols [6,16,58]. Such three-photon states can also be realized by fusing six single photons with a total probability of 1/32 [59]. With state-of-the-art SPDC sources operating at Megahertz frequencies and an extraction efficiency of $\approx 70\%$ [79], the theoretical three-photon GHZ state generation rate is in the few kilohertz regime. In comparison, using a deterministic source with the parameters of Ref. [50] we estimate a direct three-photon production rate of ≈ 5MHz [see Fig. 2(c)], which exceeds the estimate for SPDC-based method by three orders of magnitude. The fidelity of such three-photon states is $\approx 83\%$ for experimentally measured parameters, $B = 15$ [55], $\Delta = 2\pi \times 16$ GHz corresponding to a magnetic field of 2 T [55,56], $\gamma = 3.2$ ns^{-1}, and single-photon indistinguishability $I = 0.96$ [55] corresponding to $\gamma_d = 0.06$ ns^{-1} [50]. Figure 2(c) also shows the infidelity corresponding to improved experimental parameters, $B = 140$ calculated from the field

distributions of Ref. [63] for $n_g = 56$, $\Delta = 2\pi \times 64$ GHz, $\gamma_d = 0.06\ \mathrm{ns}^{-1}$ [50], and $\gamma = 5.3\ \mathrm{ns}^{-1}$ ($I = 0.98$ [37,55]).

For large entangled states the infidelity inherently grows with the system size. Hence, the relevant quantity for quantum-information applications is the infidelity per qubit. In a gate-based approach fault tolerant thresholds of 3.2% (1.4%) single qubit error has been derived for quantum computation with three-dimensional (two-dimensional) cluster states [80–82]. Potentially our deterministic generation scheme can be mapped to these setups using gates between QDs [36] or efficient Bell state measurements of photons [83]. For the parameters of Fig. 2(c), we find a comparable infidelity of 2.1% per qubit, consisting of 1.8% and 0.3% of single- and two-qubit errors, respectively. A full assessment of this possibility should take into account additional errors when extending cluster states to higher dimensions and the need for postselection but also advantages from knowing the error mechanism and the ability to do long-range interactions. This is beyond the scope of this article, but it is encouraging that the numbers we obtain for realistic experimental parameters are comparable to these requirements. The states can also be extended to higher dimensions using linear optics-based fusion, but in this case the error thresholds are more stringent [84]. Alternatively, the requirements for quantum communication protocols [85–89] are typically much more relaxed. Taking the security analysis of the anonymous transmission protocol [85] as an example, the predicted error rates are within the threshold for up to, at least, fifty parties and almost an order of magnitude below the threshold for four parties.

In conclusion, we have proposed a complete architecture of a device for scalable multiphoton entanglement generation from a QD-based emitter. Our particular implementation relies on the control of photon emission by means of nanophotonic structure, such as PCWs. Our findings predict near-future feasibility of multiphoton sources with encouraging state fidelities and generation rates compared with existing methods. The provided theoretical analysis improves our understanding of the mechanisms governing the quality of the produced states and provides a recipe for further improvement of such devices.

We gratefully acknowledge financial support from Danmarks Grundforskningsfond (DNRF 139, Hy-Q Center for Hybrid Quantum Networks), the European Research Council (ERC Advanced Grant "SCALE"), and the European Union Horizon 2020 Research and Innovation Programme under Grant Agreement No. 820445 and Project Name Quantum Internet Alliance.

[1] P. Kok, W. J. Munro, K. Nemoto, T. C. Ralph, J. P. Dowling, and G. J. Milburn, Rev. Mod. Phys. **79**, 135 (2007).
[2] M. A. Nielsen, Phys. Rev. Lett. **93**, 040503 (2004).
[3] D. E. Browne and T. Rudolph, Phys. Rev. Lett. **95**, 010501 (2005).
[4] E. Knill, R. Laflamme, and G. J. Milburn, Nature (London) **409**, 46 (2001).
[5] S. Slussarenko and G. J. Pryde, Appl. Phys. Rev. **6**, 041303 (2019).
[6] T. Rudolph, APL Photonics **2**, 030901 (2017).
[7] B. P. Lanyon, J. D. Whitfield, G. G. Gillett, M. E. Goggin, M. P. Almeida, I. Kassal, J. D. Biamonte, M. Mohseni, B. J. Powell, M. Barbieri, A. Aspuru-Guzik, and A. G. White, Nat. Chem. **2**, 106 (2010).
[8] X.-s. Ma, B. Dakic, W. Naylor, A. Zeilinger, and P. Walther, Nat. Phys. **7**, 399 (2011).
[9] G. Tóth and I. Apellaniz, J. Phys. A: Math. Theor. **47**, 424006 (2014).
[10] N. Shettell and D. Markham, Phys. Rev. Lett. **124**, 110502 (2020).
[11] K. Azuma, K. Tamaki, and H.-K. Lo, Nat. Commun. **6**, 6787 (2015).
[12] Z.-D. Li, R. Zhang, X.-F. Yin, L.-Z. Liu, Y. Hu, Y.-Q. Fang, Y.-Y. Fei, X. Jiang, J. Zhang, L. Li, N.-L. Liu, F. Xu, Y.-A. Chen, and J.-W. Pan, Nat. Photonics **13**, 644 (2019).
[13] D. Buterakos, E. Barnes, and S. E. Economou, Phys. Rev. X **7**, 041023 (2017).
[14] P. Hilaire, E. Barnes, and S. E. Economou, Quantum **5**, 397 (2021).
[15] J. Borregaard, H. Pichler, T. Schröder, M. D. Lukin, P. Lodahl, and A. S. Sørensen, Phys. Rev. X **10**, 021071 (2020).
[16] M. Pant, H. Krovi, D. Englund, and S. Guha, Phys. Rev. A **95**, 012304 (2017).
[17] J.-W. Pan, D. Bouwmeester, M. Daniell, H. Weinfurter, and A. Zeilinger, Nature (London) **403**, 515 (2000).
[18] H.-X. Lu, L.-Z. Cao, J.-Q. Zhao, Y.-D. Li, and X.-Q. Wang, Sci. Rep. **4**, 4476 (2014).
[19] M. Żukowski, Phys. Rev. A **61**, 022109 (2000).
[20] D. C. Burnham and D. L. Weinberg, Phys. Rev. Lett. **25**, 84 (1970).
[21] P. G. Kwiat, K. Mattle, H. Weinfurter, A. Zeilinger, A. V. Sergienko, and Y. Shih, Phys. Rev. Lett. **75**, 4337 (1995).
[22] A. G. White, D. F. V. James, P. H. Eberhard, and P. G. Kwiat, Phys. Rev. Lett. **83**, 3103 (1999).
[23] D. Bouwmeester, J.-W. Pan, M. Daniell, H. Weinfurter, and A. Zeilinger, Phys. Rev. Lett. **82**, 1345 (1999).
[24] A.-N. Zhang, C.-Y. Lu, X.-Q. Zhou, Y.-A. Chen, Z. Zhao, T. Yang, and J.-W. Pan, Phys. Rev. A **73**, 022330 (2006).
[25] A. Zeilinger, M. A. Horne, H. Weinfurter, and M. Żukowski, Phys. Rev. Lett. **78**, 3031 (1997).
[26] N. Kiesel, C. Schmid, U. Weber, G. Tóth, O. Gühne, R. Ursin, and H. Weinfurter, Phys. Rev. Lett. **95**, 210502 (2005).
[27] M. Zhang, L.-T. Feng, Z.-Y. Zhou, Y. Chen, H. Wu, M. Li, S.-M. Gao, G.-P. Guo, G.-C. Guo, D.-X. Dai, and X.-F. Ren, Light: Sci. Appl. **8**, 41 (2019).
[28] C.-Y. Lu, X.-Q. Zhou, O. Gühne, W.-B. Gao, J. Zhang, Z.-S. Yuan, A. Goebel, T. Yang, and J.-W. Pan, Nat. Phys. **3**, 91 (2007).
[29] X.-C. Yao, T.-X. Wang, P. Xu, H. Lu, G.-S. Pan, X.-H. Bao, C.-Z. Peng, C.-Y. Lu, Y.-A. Chen, and J.-W. Pan, Nat. Photonics **6**, 225 (2012).
[30] X.-L. Wang, L.-K. Chen, W. Li, H.-L. Huang, C. Liu, C. Chen, Y.-H. Luo, Z.-E. Su, D. Wu, Z.-D. Li, H. Lu, Y. Hu, X. Jiang, C.-Z. Peng, L. Li, N.-L. Liu, Y.-A. Chen, C.-Y. Lu, and J.-W. Pan, Phys. Rev. Lett. **117**, 210502 (2016).

[31] H.-S. Zhong, Y. Li, W. Li, L.-C. Peng, Z.-E. Su, Y. Hu, Y.-M. He, X. Ding, W. Zhang, H. Li, L. Zhang, Z. Wang, L. You, X.-L. Wang, X. Jiang, L. Li, Y.-A. Chen, N.-L. Liu, C.-Y. Lu, and J.-W. Pan, Phys. Rev. Lett. **121**, 250505 (2018).

[32] K. M. Gheri, C. Saavedra, P. Törmä, J. I. Cirac, and P. Zoller, Phys. Rev. A **58**, 2627(R) (1998).

[33] N. H. Lindner and T. Rudolph, Phys. Rev. Lett. **103**, 113602 (2009).

[34] J. P. Lee, B. Villa, A. J. Bennett, R. M. Stevenson, D. J. P. Ellis, I. Farrer, D. A. Ritchie, and A. J. Shields, Quant. Sci. Technol. **4**, 025011 (2019).

[35] M. Gimeno-Segovia, T. Rudolph, and S. E. Economou, Phys. Rev. Lett. **123**, 070501 (2019).

[36] S. E. Economou, N. Lindner, and T. Rudolph, Phys. Rev. Lett. **105**, 093601 (2010).

[37] P. Lodahl, S. Mahmoodian, and S. Stobbe, Rev. Mod. Phys. **87**, 347 (2015).

[38] I. Schwartz, D. Cogan, E. R. Schmidgall, Y. Don, L. Gantz, O. Kenneth, N. H. Lindner, and D. Gershoni, Science **354**, 434 (2016).

[39] I. Aharonovich, D. Englund, and M. Toth, Nat. Photonics **10**, 631 (2016).

[40] M. Atatüre, D. Englund, N. Vamivakas, S.-Y. Lee, and J. Wrachtrup, Nat. Rev. Mater. **3**, 38 (2018).

[41] D. D. Awschalom, R. Hanson, J. Wrachtrup, and B. B. Zhou, Nat. Photonics **12**, 516 (2018).

[42] J. H. Bodey, R. Stockill, E. V. Denning, D. A. Gangloff, G. Éthier-Majcher, D. M. Jackson, E. Clarke, M. Hugues, C. L. Gall, and M. Atatüre, npj Quantum Inf. **5**, 95 (2019).

[43] G. Kiršanskė, H. Thyrrestrup, R. S. Daveau, C. L. Dreeßen, T. Pregnolato, L. Midolo, P. Tighineanu, A. Javadi, S. Stobbe, R. Schott, A. Ludwig, A. D. Wieck, S. I. Park, J. D. Song, A. V. Kuhlmann, I. Söllner, M. C. Löbl, R. J. Warburton, and P. Lodahl, Phys. Rev. B **96**, 165306 (2017).

[44] D. Huber, M. Reindl, Y. Huo, H. Huang, J. S. Wildmann, O. G. Schmidt, A. Rastelli, and R. Trotta, Nat. Commun. **8**, 15506 (2017).

[45] M. Reindl, J. H. Weber, D. Huber, C. Schimpf, S. F. Covre da Silva, S. L. Portalupi, R. Trotta, P. Michler, and A. Rastelli, Phys. Rev. B **100**, 155420 (2019).

[46] X. Ding, Y. He, Z.-C. Duan, N. Gregersen, M.-C. Chen, S. Unsleber, S. Maier, C. Schneider, M. Kamp, S. Höfling, C.-Y. Lu, and J.-W. Pan, Phys. Rev. Lett. **116**, 020401 (2016).

[47] N. Tomm, A. Javadi, N. O. Antoniadis, D. Najer, M. C. Lbl, A. R. Korsch, R. Schott, S. R. Valentin, A. D. Wieck, A. Ludwig, and R. J. Warburton, Nat. Nanotechnol. **16**, 399 (2021).

[48] M. Arcari, I. Söllner, A. Javadi, S. Lindskov Hansen, S. Mahmoodian, J. Liu, H. Thyrrestrup, E. H. Lee, J. D. Song, S. Stobbe, and P. Lodahl, Phys. Rev. Lett. **113**, 093603 (2014).

[49] H. Wang, H. Hu, T.-H. Chung, J. Qin, X. Yang, J.-P. Li, R.-Z. Liu, H.-S. Zhong, Y.-M. He, X. Ding, Y.-H. Deng, Q. Dai, Y.-H. Huo, S. Höfling, C.-Y. Lu, and J.-W. Pan, Phys. Rev. Lett. **122**, 113602 (2019).

[50] R. Uppu, F. T. Pedersen, Y. Wang, C. T. Olesen, C. Papon, X. Zhou, L. Midolo, S. Scholz, A. D. Wieck, A. Ludwig, and P. Lodahl, Sci. Adv. **6**, eabc8268 (2020).

[51] D. M. Greenberger, M. A. Horne, and A. Zeilinger, Going beyond Bell's theorem, arXiv:0712.0921.

[52] K. Tiurev, P. L. Mirambell, M. B. Lauritzen, M. H. Appel, A. Tiranov, P. Lodahl, and A. S. Sørensen, Phys. Rev. A **104**, 052604 (2021).

[53] D. Cogan, Z.-E. Su, O. Kenneth, and D. Gershoni, A deterministic source of indistinguishable photons in a cluster state, arXiv:2110.05908.

[54] R. Vasconcelos, S. Reisenbauer, C. Salter, G. Wachter, D. Wirtitsch, J. Schmiedmayer, P. Walther, and M. Trupke, npj Quantum Inf. **6**, 9 (2020).

[55] M. H. Appel, A. Tiranov, A. Javadi, M. C. Löbl, Y. Wang, S. Scholz, A. D. Wieck, A. Ludwig, R. J. Warburton, and P. Lodahl, Phys. Rev. Lett. **126**, 013602 (2021).

[56] J. H. Prechtel, F. Maier, J. Houel, A. V. Kuhlmann, A. Ludwig, A. D. Wieck, D. Loss, and R. J. Warburton, Phys. Rev. B **91**, 165304 (2015).

[57] M. H. Appel, A. Tiranov, S. Pabst, M. L. Chan, C. Starup, Y. Wang, L. Midolo, K. Tiurev, S. Scholz, A. D. Wieck, A. Ludwig, A. S. Sørensen, and P. Lodahl, A source of indistinguishable time-bin entangled photons from a waveguide-embedded quantum dot, arXiv:2111.12523.

[58] M. Gimeno-Segovia, P. Shadbolt, D. E. Browne, and T. Rudolph, Phys. Rev. Lett. **115**, 020502 (2015).

[59] M. Varnava, D. E. Browne, and T. Rudolph, Phys. Rev. Lett. **100**, 060502 (2008).

[60] S. G. Carter, T. M. Sweeney, M. Kim, C. S. Kim, D. Solenov, S. E. Economou, T. L. Reinecke, L. Yang, A. S. Bracker, and D. Gammon, Nat. Photonics **7**, 329 (2013).

[61] S. Sun, H. Kim, G. S. Solomon, and E. Waks, Nat. Nanotechnol. **11**, 539 (2016).

[62] H. Wang, Y.-M. He, T.-H. Chung, H. Hu, Y. Yu, S. Chen, X. Ding, M.-C. Chen, J. Qin, X. Yang, R.-Z. Liu, Z.-C. Duan, J.-P. Li, S. Gerhardt, K. Winkler, J. Jurkat, L.-J. Wang, N. Gregersen, Y.-H. Huo, Q. Dai *et al.*, Nat. Photonics **13**, 770 (2019).

[63] A. Javadi, S. Mahmoodian, I. Söllner, and P. Lodahl, J. Opt. Soc. Am. B **35**, 514 (2018).

[64] P. Tighineanu, C. L. Dreeßen, C. Flindt, P. Lodahl, and A. S. Sørensen, Phys. Rev. Lett. **120**, 257401 (2018).

[65] L. Besombes, K. Kheng, L. Marsal, and H. Mariette, Phys. Rev. B **63**, 155307 (2001).

[66] E. A. Muljarov and R. Zimmermann, Phys. Rev. Lett. **93**, 237401 (2004).

[67] A. Thoma, P. Schnauber, M. Gschrey, M. Seifried, J. Wolters, J.-H. Schulze, A. Strittmatter, S. Rodt, A. Carmele, A. Knorr, T. Heindel, and S. Reitzenstein, Phys. Rev. Lett. **116**, 033601 (2016).

[68] D. V. Bulaev and D. Loss, Phys. Rev. Lett. **95**, 076805 (2005).

[69] A. V. Khaetskii, D. Loss, and L. Glazman, Phys. Rev. Lett. **88**, 186802 (2002).

[70] X. Hu, R. De Sousa, and S. D. Sarma, Decoherence and dephasing in spin-based solid state quantum computers, in *Foundations of Quantum Mechanics in the Light of New Technology* (World Scientific, Singapore, 2002), pp. 3–11.

[71] F. H. L. Koppens, K. C. Nowack, and L. M. K. Vandersypen, Phys. Rev. Lett. **100**, 236802 (2008).

[72] L. Huthmacher, R. Stockill, E. Clarke, M. Hugues, C. Le Gall, and M. Atatüre, Phys. Rev. B **97**, 241413(R) (2018).

[73] D. Press, K. De Greve, P. L. McMahon, T. D. Ladd, B. Friess, C. Schneider, M. Kamp, S. Höfling, A. Forchel, and Y. Yamamoto, Nat. Photonics **4**, 367 (2010).

[74] H. Jayakumar, A. Predojević, T. Kauten, T. Huber, G. S. Solomon, and G. Weihs, Nat. Commun. **5**, 4251 (2014).
[75] A. Bechtold, D. Rauch, F. Li, T. Simmet, P.-L. Ardelt, A. Regler, K. Müller, N. A. Sinitsyn, and J. J. Finley, Nat. Phys. **11**, 1005 (2015).
[76] H. Pichler, S. Choi, P. Zoller, and M. D. Lukin, Proc. Natl. Acad. Sci. U.S.A. **114**, 11362 (2017).
[77] W. Sheng, Appl. Phys. Lett. **96**, 133102 (2010).
[78] J. Houel, J. H. Prechtel, A. V. Kuhlmann, D. Brunner, C. E. Kuklewicz, B. D. Gerardot, N. G. Stoltz, P. M. Petroff, and R. J. Warburton, Phys. Rev. Lett. **112**, 107401 (2014).
[79] F. Kaneda and P. G. Kwiat, Sci. Adv. **5**, eaaw8586 (2019).
[80] R. Raussendorf, J. Harrington, and K. Goyal, Ann. Phys. (NY) **321**, 2242 (2006).
[81] R. Raussendorf and J. Harrington, Phys. Rev. Lett. **98**, 190504 (2007).
[82] R. Raussendorf, J. Harrington, and K. Goyal, New J. Phys. **9**, 199 (2007).
[83] D. Witthaut, M. D. Lukin, and A. S. Sørensen, Europhys. Lett. **97**, 50007 (2012).
[84] S. Bartolucci, P. Birchall, H. Bombin, H. Cable, C. Dawson, M. Gimeno-Segovia, E. Johnston, K. Kieling, N. Nickerson, M. Pant, F. Pastawski, T. Rudolph, and C. Sparrow, Fusion-based quantum computation, arXiv:2101.09310.
[85] V. Lipinska, G. Murta, and S. Wehner, Phys. Rev. A **98**, 052320 (2018).
[86] M. Christandl and S. Wehner, *Advances in Cryptology: ASIACRYPT 2005*, edited by B. Roy (Springer, Berlin, 2005), pp. 217–235.
[87] G. Brassard, A. Broadbent, J. Fitzsimons, S. Gambs, and A. Tapp, *Advances in Cryptology: ASIACRYPT 2007*, edited by K. Kurosawa (Springer, Berlin, 2007), pp. 460–473.
[88] M. Hillery, V. Bužek, and A. Berthiaume, Phys. Rev. A **59**, 1829 (1999).
[89] A. Ambainis, H. Buhrman, Y. Dodis, and H. Röhrig, *Proceedings of the 19th Annual IEEE Conference on Computational Complexity, Amherst, MA, 2004* (IEEE, Piscataway, NJ, 2004), p. 250.